ACS APPLIED MATERIALS & INTERFACES

Research Article

www.acsami.org

Highly Efficient and Flexible Electrospun Carbon–Silica Nanofibrous Membrane for Ultrafast Gravity-Driven Oil–Water Separation

Ming Hang Tai,[†] Peng Gao,[†] Benny Yong Liang Tan,[†] Darren D. Sun,*[,†] and James O. Leckie[‡]

[†]School of Civil and Environmental Engineering, Nanyang Technological University, Singapore 639798

[‡]Department of Civil and Environmental Engineering, Stanford University, Stanford, California 94305-4020, United States

Supporting Information

ABSTRACT: A novel free-standing and flexible electrospun carbon–silica composite nanofibrous membrane is newly introduced. The characterization results suggest that the electrospun composite nanofibers are constructed by carbon chains interpenetrated through a linear network of 3-dimensional SiO_2. Thermogravimetric analysis indicates that the presence of insulating silica further improve the thermal resistance of the membrane. Additionally, the mechanical strength test shows that the membrane's toughness and flexibility can be enhanced if the concentration of SiO_2 is maintained below 2.7 wt %. Thermal and chemical stability test show that the membrane's wettability properties can be sustained at an elevated temperature up to 300 °C and no discernible change in wettability was observed under highly acidic and basic conditions. After surface-coating with silicone oil for 30 mins, the composite membrane exhibits ultra-hydrophobic and superoleophilic properties with water and oil contact angles being 144.2 ± 1.2° and 0°, respectively. The enhanced flexibility and selective wetting property enables the membrane to serve as an effective substrate for separating free oil from water. Lab-scale oil–water separation test indicates that the membrane possesses excellent oil–water separation efficiency. In addition, its inherent property of high porosity allows oil–water separation to be performed in a gravity-driven process with high-flux. We anticipate that this study will open up a new avenue for fabrication of free-standing carbonaceous composite membrane with tunable flexibility for energy efficient and high-throughput production of clean water.

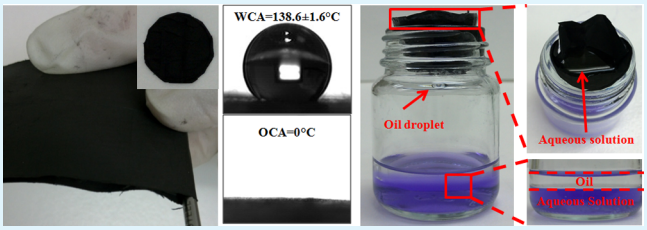

KEYWORDS: *electrospinning, silica, carbon nanofiber, flexibility, superoleophilicity, membrane, oil–water separation*

INTRODUCTION

With increasing industrial oily wastewater and stringent regulations on its discharge limit, effective separation of oil–water mixtures at low cost becomes a worldwide challenge. In addition to low cost, it is also desirable for an oil–water separation medium to possess properties, such as selective wetting behavior, high-throughput production of clean water, easy regeneration and reusability. In general, fabrication of material with selective wetting property can be achieved via modification of its surface geometry (e.g. design of hierarchical roughness at two different length scales)[1−5] and surface chemical composition (e.g. fluorine-based coating).[6−10] For instance, Ma et al.[11] reported the superhydrophobic function of an electrospun nonwoven fibrous mat prepared by decorating micrometer-scale fibers with nanometer sized particles. Apart from that, by employing in-situ polymerization of fluorinated monomer, Tang et al.[12] have endowed a hydrophilic electrospun nanofibrous membrane with superhydrophobic and superoleophilic property. In addition to selective wettability, it is equally important for the substrate to be highly porous to achieve a high throughput. This is because a highly porous structure will greatly affects the permeation rate across the membrane. In this regard, electrospinning offers a promising way to fabricate nonwoven fibrous mats with high porosity and controllable thickness.

Presently, several techniques[13−17] have been developed to perform effective oil removal process. A notable example is the gravity-driven separation on a hierarchically structured or coated mesh. The mesh surface is either coated with low surface energy material[18−21] or composed of micro/nano-hierarchical structure[22−24] to impart desirable wetting property. One major merit from using mesh for oil–water separation is its ultrafast separation rate. Membrane-based separation of oil–water[25−27] under pressure is a widely used techniques in industries because of the high quality water produced, simple modular design, and lower chemical consumption compared to other treatments.[28] However, the pressure-driven membrane separation has a major drawback–fouling.[29−31] Under high trans-membrane pressure difference, oil droplets depositing on the membrane surface are deformed and forced to enter the pores. As a consequence, the pores are blocked and water flow rate is decreased. Therefore, it is expected that a membrane separation at low pressure will be a preferred and more sustainable approach. Apart from fouling problem, the regeneration of oil-fouled membrane is also a great challenge. In practice, the cleaning of fouled membrane requires harsh

Received: March 25, 2014
Accepted: May 13, 2014
Published: May 13, 2014

   dx.doi.org/10.1021/am501758c | ACS Appl. Mater. Interfaces 2014, 6, 9393−9401

chemical conditions or involves high-temperature thermal treatment, which is detrimental to the membrane that is low in thermal and chemical resistance such as polymer membrane. Therefore, search for chemically and thermally stable membrane becomes imperative.

Carbonaceous nanomaterials, such as carbon nanotube and carbon nanofiber (CNF), are well known for its excellent thermal stability[32,33] and chemical inertness.[34] Because of its inherent property of hydrophobicity and oleophilicity, carbonaceous materials have been deemed as a promising candidate for oil sorption and oil−water separation.[35,36] A great advantage that carbonaceous nanomaterials offer in such applications is that it allows easy regeneration after use because of its high thermal and chemical stability. However, carbonaceous materials often suffer from low rigidity when they are assembled into macrostructure. This largely restricts its performance in the relevant applications. For practical usage, the material must be flexible to withstand the physical impact during the process of oil sorption or oil-water separation. While majority of studies works on carbon nanotubes and its 3-dimensional (3D) assemblies for oil-water separation, the study of using continuous CNFs in the form of nonwoven mat or membrane for oil−water separation is still absent.

Hence, in this contribution, we discuss the fabrication of highly flexible carbon-based composite nanofibrous membrane via addition of SiO_2 precursor and the resulting membrane's physical properties including bulk mechanical strength and thermal stability. The performance of the fabricated membrane on gravity-driven separation of oil−water mixtures is also evaluated. We seek to show that the as-fabricated electrospun carbonaceous composite membrane is able to separate effectively oil−water at high flux and work efficiently over a broad range of temperature and pH levels.

EXPERIMENTAL SECTION

Preparation of SiO_2−Carbon Composite Nanofibers. The spin dope for SiO_2−carbon composite was prepared by mixing polyacryonitrile (PAN, MW = 150 000 g/mol, 7 wt %) and tetraethyl orthosilicate (TEOS, 0.5−5 wt %) in a mixture solvent of dimethylformamide (DMF)/acetic acid (volume ratio of 15/1). TEOS was used as an alkoxide precursor of SiO_2 while PAN serves as both a carrying polymer for TEOS and a precursor of carbon nanofiber (CNF). Glacial grade acetic acid was added to acidify the mixture while ensuring low water/TEOS ratio. The mixture was then heated at 90 °C until a crystal clear solution was obtained. Following this, the prepared spin dope was electrospun in a closed chamber where the electric field strength was kept at approximately 0.6−0.8 kV/cm. The solution feeding rate was 9−10 μL/min. The SiO_2−PAN nanofibrous mat was collected by using a rotating drum and the as-spun mat was left in air overnight for further hydrolysis despite that the moisture in air could engender the hydrolysis during the electrospinning. To prevent the nozzle blockage by the rapidlly hydrolyzed spin dope, a solvent vapor jacket is designed and used to cover the spinneret, as shown in Supporting Information Figure S1.

The collected sheets of SiO_2−PAN fibrils were then oxidized (stabilized) at 280 °C in air for 2 h and carbonized at 900 °C in nitrogen for 2 h. In both processes, the ramping rate was kept at 3 °C/min. The pure SiO_2 nanofibers can be obtained by heating at 550 °C in air for 2 h at a ramping rate of 8 °C/min to remove the carbon framework. For comparison, pure carbonaceous nanofibers were also fabricated. Throughout the experiments, the PAN content in the spin dopes was fixed at 7 wt %.

Characterization. The surface morphology of the as-fabricated samples was analyzed by field emission scanning electron microscopy (FESEM, JEOL JSM-7600F). Transmission electron microscopy (TEM) images were obtained by using a JEOL 2010-H microscope operating at 200 kV. The crystal phase of the samples were confirmed by X-ray diffraction (XRD, Shimadzu XRD-6000) with monochromated high-intensity Cu Kα radiation (λ = 1.5418 Å) operated at 40 kV and 30 mA. Elemental mapping was performed by using energy-dispersive X-ray spectroscopy (EDX, Oxford Instruments X-max). The membranes' oxidation resistance was determined by performing thermogravimetric (TG) analysis (Perkin Elmer TGA-7) where the sample was heated from 30 to 900 °C at a rate of 10 °C/min and was immediately cooled down after reaching the pre-determined temperature.

Mechanical Strength Test. The Young's modulus of a single SiO_2-carbon composite nanofiber and CNF was evaluated by carrying out atomic force microscopy (AFM, Park Systems XE-100) based on the method of Kracke and Damaschke.[37−39] In this work, a PPP-NCHR silicon cantilever with 169 GPa modulus and force constant of 42 N/m was employed. The cantilever has a pyramidal tip with contact radius <10 nm. During the experiment, the samples were placed on a stainless steel spherical holder. The force mapping on the fiber surface was done from a randomly selected area of 5 × 5 μm^2. To derive the Young's modulus, the relationship between the fiber nanoindentation and the force applied was utilized which is given by $dF/d\delta = (2/\pi^{0.5})E \times A^{0.5}$ where A is the contact area and E^* the effective Young's modulus, defined as $1/E^* = 1 - \upsilon_{tip}^2/E_{tip} + 1 - \upsilon_{sample}^2/E_{sample}$, where υ is the Poisson ratio.

To measure bulk mechanical strength, tensile strength test was conducted by using Instron 5567 computerized universal testing machine. Throughout the test, 1 × 5 cm samples with crip length of 2 cm were clamped and pulled at a rate of 0.2 mm/min. For each sample, a stress−strain curve could be obtained and used for toughness measurement (by integrating the area under the stress−strain curve).

Qualitative Analysis of Oil−Water Separation Efficiency. Silicone oil-coated SiO_2−carbon composite membrane was used as separation medium and a mixture of petroleum spirit and 0.2 M hydrochloric acid (HCl) aqueous solution (dyed with methyl violet) was prepared. Prior to the separation test, the flexible membrane was folded to fit in the opening of a vial containing 0.2 M silver nitrate ($AgNO_3$) aqueous solution which is dyed with methyl violet. The addition of methyl violet to the HCl and $AgNO_3$ aqueous solution could result in different colors due to the difference in pH. In an acidic solution (pH <1.6), methyl violet appears to be yellowish and it is turned into blue-violet when the pH value rises above 1.6. Hence, the as-prepared HCl and $AgNO_3$ aqueous solution gave rise to yellowish and blue-violet, respectively. The as-prepared oil-water mixture was then poured into the vial through the coated composite membrane. Because of its high sensitivity to Cl^- ions, the $AgNO_3$ aqueous solution in the vial can serve as an indicator in a manner that it reacts with HCl to immediately form whitish AgCl precipitate (solubility product, $K_{sp} = 1.8 \times 10^{-10}$). Hence, even a minuscule amount of HCl aqueous solution penetrating through the membrane will be detected. By observing the formation of AgCl precipitates, the membrane's separation efficiency can be qualitatively determined. The separation performance was conducted under two pouring conditions, that is, water was added immediately followed by oil and vice versa and the membrane used were initially dry.

RESULTS AND DISCUSSION

Figure 1a shows the FESEM images of as-spun SiO_2−carbon composite nanofibers prepared from 5 wt % TEOS. It can be seen that the membrane is composed of entangled nanofibers with an average diameter of 481 ± 57 nm based on 150 fiber measurement. This highly dense fiber entanglement leads to the formation of 3D macroporous network which could facilitate the liquid permeation rate across the membrane because of the decreased mass transfer resistance. The enlarged image in Figure 1b reveals that the nanofiber has a rough surface with wrinkles. The formation of wrinkles is probably due to the competition between the phase separation and the fast evaporation rate of the DMF solvent in solution jet during

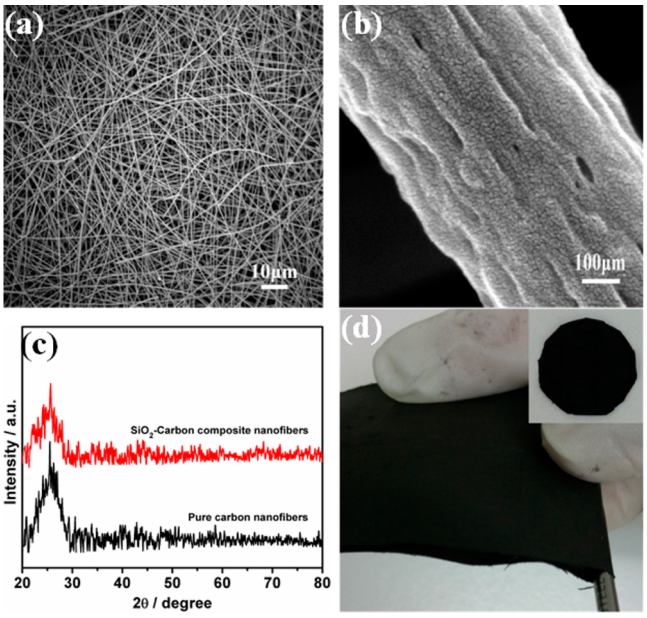

Figure 1. Characterization of electrospun composite nanofibers. (a) Top view of electrospun composite nanofibrous mat. (b) Surface morphology of a single composite nanofiber. (c) XRD pattern showing amorphous carbon and silica in pristine CNFs and the composite nanofibers. (d) Flexibility of the composite nanofibrous mat, which can be easily cut into desirable shape, as shown in the inset.

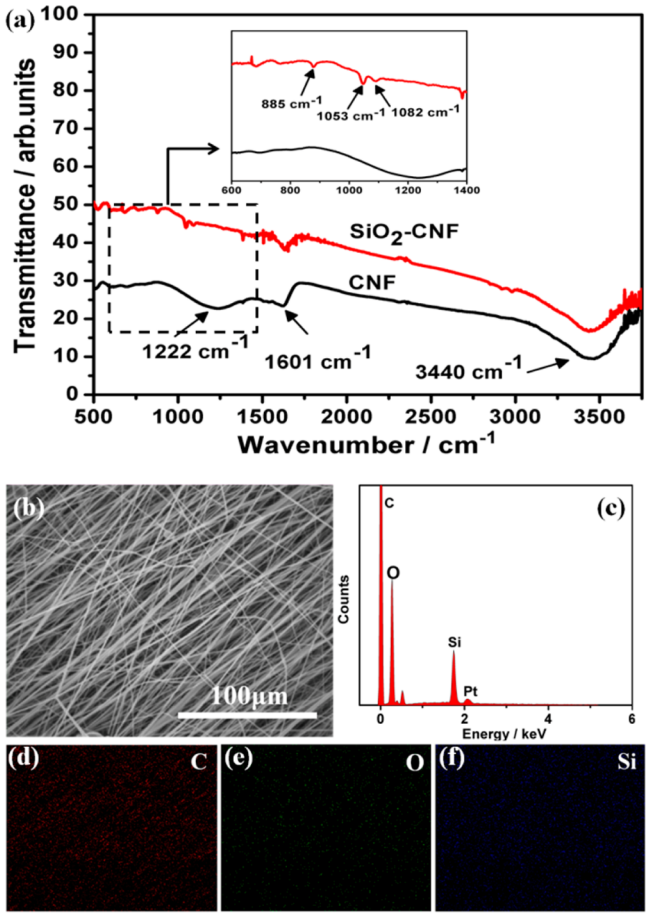

Figure 2. (a) FTIR spectra of the as-prepared CNFs and SiO_2–carbon composite nanofibers. Elemental maps. (b) FESEM image of SiO_2–carbon composite nanofibers. (c) EDX spectrum and (d) carbon, (e) oxygen, and (f) silicon maps of SiO_2–carbon composite nanofibers taken in panel b.

the electrospinning process. It is interesting to note that, the fiber-like morphology of the composite is still preserved even after the carbon is removed by calcination at 550 °C (see Supporting Information Figure S2) The calcination also turns the nanofibers from black into white. This suggests that the SiO_2 present in the composite forms a linear network. XRD pattern of both pristine CNFs and SiO_2–carbon composite nanofibers, as seen in Figure 1c, show broad diffraction peaks at approximately 25°, suggesting that the phase of carbon and SiO_2 is amorphous. It is noteworthy that the characteristic peak for both amorphous carbon and SiO_2 are close to each other (~23–25°)[40–42] and the diffraction peak of carbon overlaps that of SiO_2 in this case. This explains why the XRD spectrum of SiO_2–carbon composite nanofibers shows only one diffraction peak which appeared to be similar to the pristine CNFs. TEM examination further confirms the amorphous phase of SiO_2 in the composite nanofibers (Supporting Information Figure S3). Figure 1d demonstrates that the composite nanofibrous membrane can be bent to a radius curvature of 1.5 mm without any cracks. The membrane can be even severely folded. Because of its excellent flexibility, the membrane can be readily cut into desired shape as shown in the inset of Figure 1d. The membrane flexibility and its corresponding mechanical properties will be further discussed in a later section.

Figure 2a shows the FTIR spectra of pristine CNFs and SiO_2-carbon composite nanofibers. For CNFs, the spectrum shows the characteristic peaks at ~1222 and 1601 cm^{-1} which correspond to the C=C stretching and bending vibrations of the carbon backbone, respectively. The broad peak at 3100–3700 cm^{-1} can be assigned to the N–H bonds.[43] However, the peak at 3440 cm^{-1} belongs to the asymmetrical stretching vibration of O–H groups because of the water adsorbed on the surfaces.[44] After the addition of TEOS, the resultant composite nanofibers show new peaks of Si–O stretching and bending vibrations at ~1082 and 1053 cm^{-1}, respectively. The peak at 885 cm^{-1} is ascribed to the silanol (Si–OH) vibration.[45] The detection of Si–O indicates the formation of SiO_2 in the fibers. No Si–C bond is observed, suggesting that there is lack of intermolecular interaction between the silica and the carbon species in the composite system and they form interpenetrating structure separately during their transformation.[46] It is noted that, although most of Si–OH groups can be removed by dehydroxylation at elevated temperature during the carbonization process, the detected Si–OH can be attributed to the isolated single silanols remained on the silica surface.[47]

To verify the presence of silica in the fibers, the composition of CNF sample containing 5 wt % Si precursor was further characterized by EDX as shown in Figure 2b–f. The results from the EDX analysis confirms that the composite nanofibers are mainly composed of Si, O, and C. These are indicated by the strong peaks in the EDX spectrum. In addition, it can be seen that the Si element is evenly distributed across the surface of the nanofibers as shown in Figure 2f.

On the basis of the experimental results, the formation mechanism of SiO_2–carbon composite nanofibers is proposed and illustrated in Figure 3. Prior to electrospinning, the sol–gel precursor is prepared by mixing PAN, TEOS, DMF, and acetic acid. During the process where the precursor sol is spun into fibers under appropriate electrical strength, phase separation

dx.doi.org/10.1021/am501758c | ACS Appl. Mater. Interfaces 2014, 6, 9393–9401

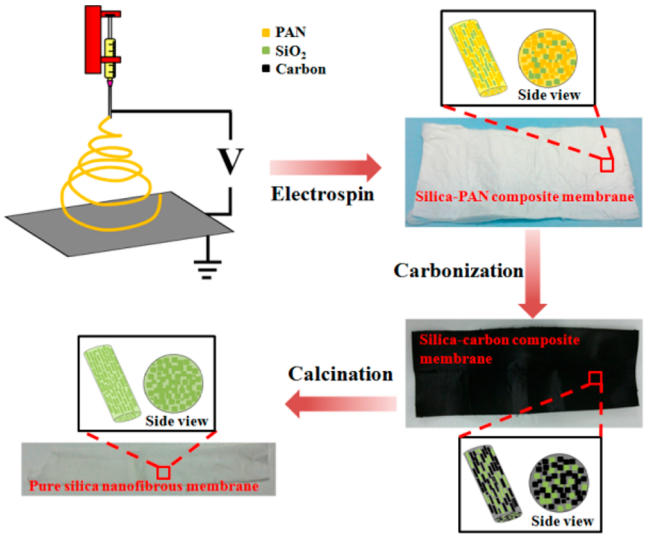

Figure 3. Schematic of fabricating silica–PAN composite membrane, silica–carbon composite membrane, and pure silica nanofibrous membrane by employing electrospinning technique.

takes place. The DMF solvent in the precursor evaporates quickly from the fiber in the meantime PAN the TEOS undergoes hydrolysis. The surface morphology of the electrospun fibers is the result of the competition between phase separation dynamics and evaporation rate of DMF solvent in solution jet during electropinning. During the hydrolysis, TEOS is polycondensed to form SiO_2 linear framework instead of SiO_2 colloidal particles owing to the fact that the rate of condensation is slow relative to the rate of hydrolysis under the acidic catalysis.[48,49] Consequently, the resultant composite nanofibers is a continuous PAN phase with homogeneously dispersed, phase separated SiO_2 domains. Upon carbonization at elevated temperature under inert atmosphere, the PAN phase is converted into carbon phase. The process also leads to complete condensation of hydrolyzed TEOS to SiO_2.[45] The final state of SiO_2 in the composite is remained as evidenced from the broad band diffraction peak at 2θ values of approximately 25° in the XRD spectra in Figure 1c. It is noted that the morphology and integrity of the composite nanofibers is well-retained after carbonization despite that carbon and silica have different shrinkage rates. This is owing to the interpenetration framework of carbon and SiO_2 which allows the shrinkage to be engendered in a homogenous manner.[46] After removing carbon framework through calcination, pure whitish SiO_2 nanofibers can be obtained. However, the resultant SiO_2 nanofibers are very fragile because predominant volumetric fraction of the composite is occupied by carbon and its removal renders the nanofibers mechanically weak.

The percentage of the silica component in the composite nanofibers can be derived from thermogravimetric (TG) analysis. The TG curves shown in Figure 4a indicate that the addition of 0.5, 1, 3, and 5 wt % TEOS resulted in SiO_2 loading of 2.7, 3.2, 8.5, and 15.8 wt %, respectively, in the composite fibers. With increasing SiO_2 loading, the thermal stability of the composite nanofibers is remarkably enhanced. It is observed that the maximum temperature at which the composite fibers are oxidized shifted toward higher temperature region. Apart from that, the weight loss rate is decreased. Compared to the pure CNFs, the composite nanofibers exhibits less steep weight loss and stabilized at higher temperature. Among the samples,

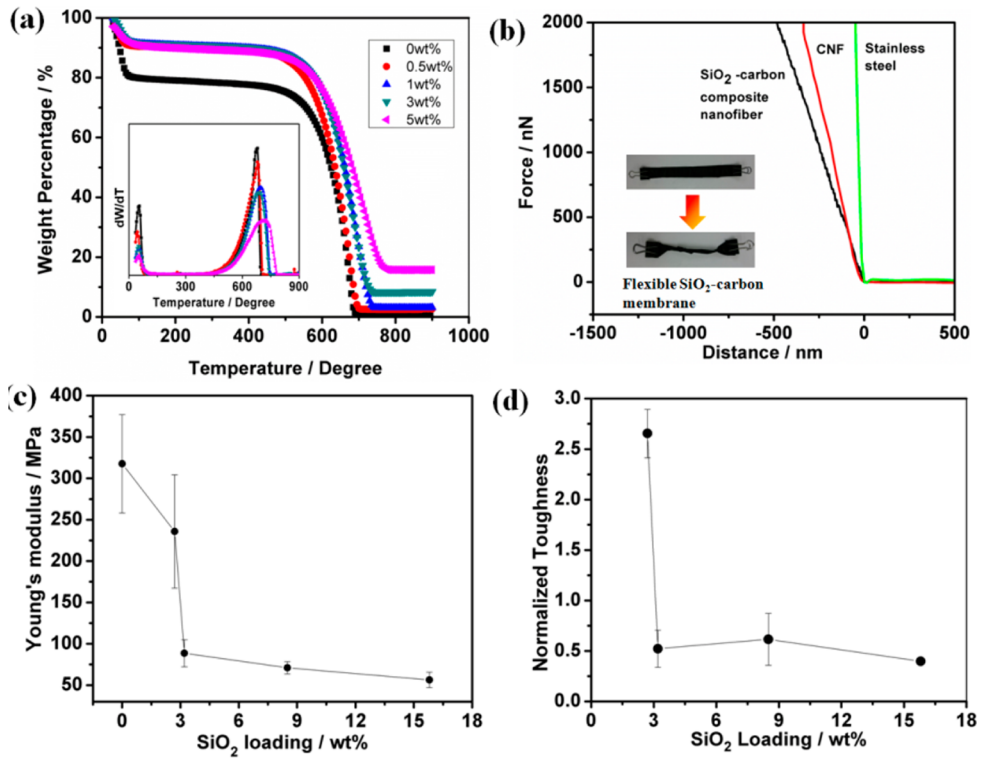

Figure 4. Effect of SiO_2 loading. (a) TG analysis result showing the enhanced thermal stability with increasing SiO_2 content. (b) Relative difference in flexibility between a single CNF and SiO_2–carbon composite nanofiber. Inset shows the excellent flexibility of the composite membrane. Plots of (c) Young's modulus and (d) normalized toughness as a function of SiO_2 loading.

dx.doi.org/10.1021/am501758c | ACS Appl. Mater. Interfaces 2014, 6, 9393–9401

15.8 % SiO_2−carbon composite nanofibers have the lowest weight loss rate and stabilize at the highest temperature. The inset of Figure 4a shows the maximum oxidation rate derived by taking the first derivative of the TG curves. As seen, the onset of maximum oxidation rate (the highest peak in the differential curve) is delayed with increasing SiO_2. The maximum oxidation rate for 15.8 wt % SiO_2−carbon composite nanofibers occurs at 720 °C. This enhancement in thermal stability could be attributed to the thermal insulation effect of silica in the composite fibers.[50]

The mechanical property of a single CNF and 15.8 wt % SiO_2−carbon composite nanofibers was studied by using AFM in contact mode. The force applied after the tip contacts with the sample and the force required to pull off from the sample surface can provide a measurement of stiffness. Seventeen force−distance (F−D) curves for each samples were collected from a randomly selected area of the sample, which was placed on a stainless steel substrate. Figure 4b shows the representative F−D curves of the electrospun CNF, the SiO_2−carbon composite nanofibers and stainless steel (as standard). The relative difference in Young's modulus CNF and SiO_2−carbon composite nanofiber can be estimated from the slope of the force-indentation curve by using the approach as described in the Experimental Section. The calculation shows that SiO_2−carbon composite nanofiber has an average Young's modulus about 3 times lower than that of CNF, suggesting that SiO_2−carbon composite nanofiber is more flexible than CNF. It is observed that the membrane flexibility can be manipulated by tuning the SiO_2 content in the composite nanofibers. This enhanced flexibility can be confirmed by manually twisting the membrane. As seen in the inset of Figure 4b, the membrane could be severely twisted without breaking. After twisting, the membrane could recover very quickly to its initial state without causing structural deformation. On the contrary, the pure CNF membrane was brittle and quickly broke into pieces after folding. (see more in Supporting Information video S1)

To further study the effect of silica, tensile test was conducted on the fabricated membranes with different SiO_2 loading. As seen in Figure 4c, the Young's modulus is decreased with increasing SiO_2 concentration. At 15.8 wt % SiO_2 concentration, the Young's modulus of the membrane is dropped from 317.6 to 56.3 MPa or by 82.3 %. However, the membrane toughness is increased followed by a steep drop, which occurs after a threshold concentration (2.7 wt %) is reached. The drop in membrane toughness suggests that the strengthening effect of silica is only effective when its concentration is maintained below 2.7 or 0.5 wt % TEOS loading. Since there is weak interactions between the carbon matrix and the silica as evidenced from FTIR analysis, silica, in this case, acts as a nonreactive and nonreinforcing filler. When an external stress is applied to the composite nanofiber, it is transferred from the carbon matrix to the embedded SiO_2 which deflects the crack propagation on the carbon matrix and consequently the stress concentration at the crack tips is reduced, thus preventing the structural failure.[51] However, as the SiO_2 content increased to a concentration above 2.7 wt %, the membrane toughness decreased substantially. This can be attributed to the agglomeration of SiO_2, which becomes a flaw to the composite nanofibers rather than a crack deflector.

The membrane flexibility was further examined under harsh condition. To do so, the membrane was immersed in liquid nitrogen (−196°C) for seconds before it was taken out and folded. For comparison, a similar test was conducted to commercial cellulose acetate (CA) membrane. It is found that the CA membrane was very brittle and could be easily break apart a few seconds after it was taken out from the liquid nitrogen. On the contrary, the SiO_2−carbon composite nanofibrous membrane remained highly flexible even after several time of immersion and folding, thus implying its high durability at super low temperature. (see Supporting Information video S2) This excellent flexibility under harsh conditions helps to maintain the structural integrity of the composite membrane during the oil-water separation process as will be discussed in the later section. Moreover, the approach to preparing flexible carbon-based membrane through silica addition provides a solution to the carbon brittleness which is normally alleviated through optimizing the precursors and preparation method.

To examine the wetting behavior, water contact angle (WCA) and oil contact angle (OCA) were measured by dropping 3 μL water (72.1 mN m^{-1}) and oil (dichloromethane, 35.4 mN m^{-1}) onto the fabricated composite membrane. As shown in Figure 5, the membrane displays a WCA of 138.6 ± 1.6° and OCA close to 0°, indicating its ultrahigh hydrophobic and superoleophilic character. This is under expectation because carbonaceous materials are intrinsically hydrophobic. However, it was observed at some locations of the membrane that the water droplet was shape-unstable and rapidly absorbed by the membrane within several seconds. The absorption process is illustrated in Supporting Information Figure S4. In other words, at these particular locations, the surfaces are superamphiphilic. This nonhomogeneity in surface wettability is probably a consequence of the competition between the natural hydrophobic effect and the porosity-driven hydrophilicity. It has been reported that porous materials such as silica thin film and methyltriethoxysilane sol−gel foam is more likely to display hydrophobic to hydrophilic switching.[52,53] Therefore, it is speculated that the observed wetting transition is engendered by the high porosity of the composite membrane that drives water infiltrate into the 3D fibrous network. To improve its hydrophobicity property and ensure homogeneous hydrophobic−oleophilic surface pattern, the membrane was coated with silicone oil at 125 °C for 0.5 h by mean of vapor deposition. Upon heat treatment, silicone oil is thermally degraded and the vaporized molecules deposit homogeneously

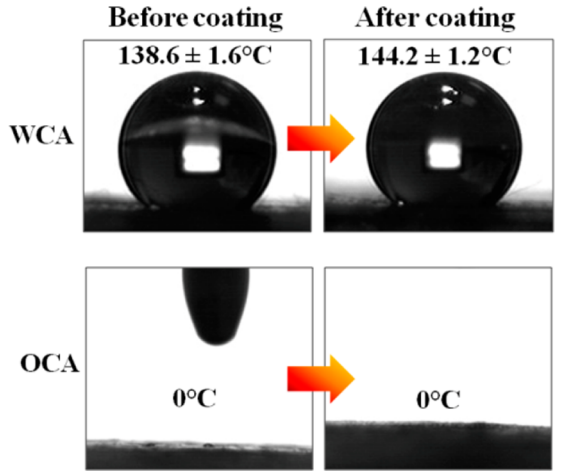

Figure 5. Hydrophobicity and oleophilicity property of the composite membrane before and after silicone oil coating.

on the nanofiber surface. After coating, the membrane exhibits WCA of 144.2 ± 1.2°, which is slightly higher than the untreated one while the membrane superoleophilicity is sustained at an OCA close to 0°.

Chemical stability test was performed to evaluate the effect of pH to the membrane's wettability. As seen in Figure 6a, the membrane could maintain ultrahigh hydrophobicity towards a broad range of pH (2−14), suggesting its excellent stability against extreme pH condition. This implies that the membrane is superior over those polymeric membranes. The membrane's hydrophobicity after calcination for 2 h at various temperatures (100−400 °C, ramping rate of 5 °C/min) was also studied. As shown in Figure 6b, the hydrophobicity is maintained after annealing treatment up to 350 °C. At 400 °C, the membrane was reduced to its initial state and lost its constancy of hydrophobicity which can be manifested by the substantial drop in WCA close to 0°. Several implications can be drawn from the chemical and thermal stability test. Firstly, the membrane wettability is switchable between hydrophobic and hydrophilic states by coating the surface with hydrophobic/hydrophilic materials that can be removed at elevated calcination temperature. Secondly, with stable hydrophobicity at high temperature (300 °C), the membrane should be able to serve effectively as a separation medium under high temperature condition such as oil spill incidents accompanied by a great fire due to burning of oil spill. Thirdly, the oil-fouled membrane can be easily regenerated and reused by means of calcination and chemical cleaning.

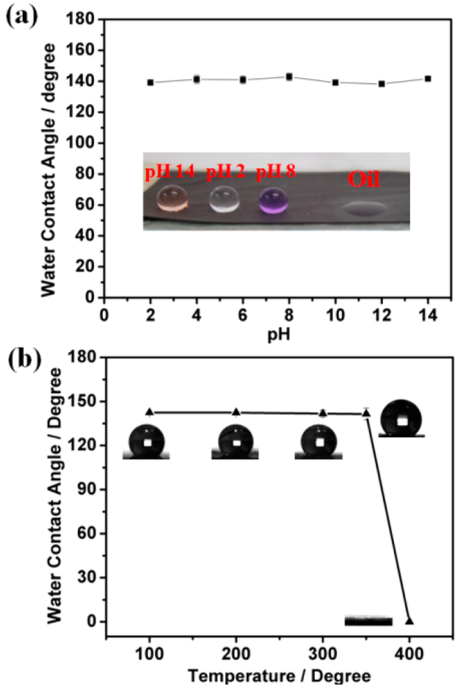

Figure 6. Study of stability of the SiO_2−carbon composite membrane. (a) WCAs when exposed to aqueous solutions with different pHs. Inset shows the ultrahigh hydrophobicity at different pHs and superoleophilicity of the membrane. (b) Variation of WCAs after calcination at various temperatures for 2 h. Inset figures show water shape at different temperatures.

The characteristic of high porosity coupled with selective wettability makes the SiO_2−carbon composite membrane a promising material for oil−water separation. As a proof of concept, the gravity-driven oil-water separation experiment was conducted and the separation performance was evaluated qualitatively. A mixture of petroleum spirit (colorless) and 0.2 M HCl aqueous solution (yellowish) was prepared and poured slowly onto the coated membrane which is flexible enough to be fitted into the opening of a vial as shown in Figure 7a and c. The vial was pre-filled with 0.2 M $AgNO_3$ aqueous solution (violet) which was used to detect the HCl that penetrated through the membrane. Owing to the fact that Ag^+ is highly sensitive to Cl^- ions, even a tiny amount of HCl will react with $AgNO_3$ to form whitish precipitate. As seen in Figure 7b, whitish precipitate was immediately formed after a 5 μL droplet of HCl was added into $AgNO_3$ solution. However, when petroleum spirit was added onto the membrane immediately followed by HCl solution, the solution in the vial remained as clear as before after the oil-water separation, as seen in Figure 7c. Only HCl aqueous solution was retained on the membrane. The separation performance was remained unaltered even when HCl solution was first poured followed by petroleum spirit. (see Supporting Information Video S3) These indicate that the coated membrane can separate oil from water efficiently regardless the pouring conditions.

Apart from the excellent separation performance, the membrane also allows ultrafast oil−water separation by solely gravity. The fluxes of various oils permeating through a membrane are measured and the flux test was repeated 3 times to obtain average values. The average permeate flux for

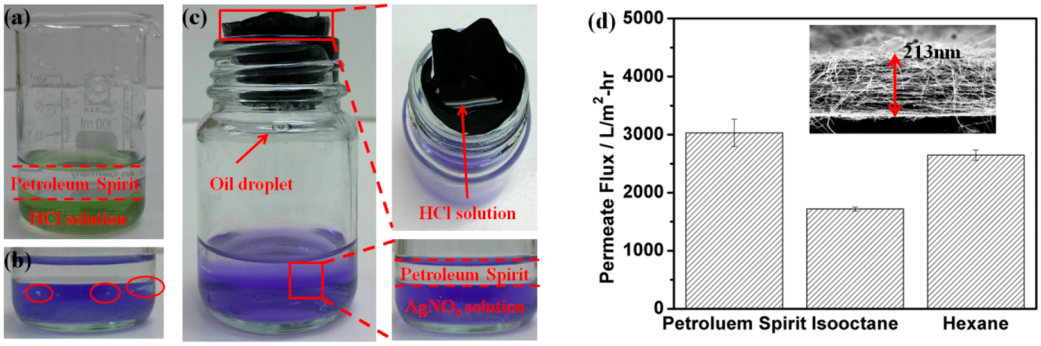

Figure 7. Ultrafast gravity-driven oil−water separation. (a) Mixture of petroleum spirit and HCl aqueous solution as feed. (b) Whitish AgCl precipitate formed after HCl reacts with $AgNO_3$ solution (violet). (c) Demonstration of gravity-driven oil−water separation. Enlarged pictures show that water is completely retained on the membrane surface and no AgCl precipitate is formed during the separation. (d) Permeate flux for different types of oils. The inset shows the cross-sectional view of the membrane thickness.

petroleum spirit, iso-octane, and hexane was found to be 3032.4 ± 234.6, 1719.1 ± 36.2, and 2648.8 ± 89.7 L/m^2-h, respectively when a 213.3 ± 21.8 μm thick membrane (effective membrane area is 0.000962 m^2) was used (Figure 7d). These values are comparable to or even higher than other advanced filtration membranes such as mineral-coated polypropylene microfiltration membrane (>2000 L/m^2-h),[54] superhydrophobic polyvinylidene fluoride membrane (700−3500 L/m^2-h)[55] and crosslinked poly(ethylene glycol) diacrylate-coated membrane (<100 L/m^2-h).[57] The variations in flux for different oils are due to the viscosity difference. According to the Haigen-Poiseuille equation, flux is inversely proportional to liquid viscosity. The viscosity for petroleum spirit, iso-octane and hexane is 0.3, 0.5, and 0.3 mPa.s, respectively. Such fast mass transport could be attributed to both the superoleophilic surface as well as the open, interconnected pore structure of the membrane which substantially decrease the mass transfer resistance. When compared to the conventional pressure-driven filtration membranes such as polymeric flat-sheet,[57] hollow fiber membrane[27] and ceramic membrane,[58] the use of electrospun carbon−silica membrane for oil−water separation is advantageous because (1) it is energy efficient (separation by gravity), (2) significantly high permeate fluxes of 1500−3000 L/m^2-h can be achieved (i.e. high throughput production), and (3) it is able to work effectively under harsh conditions such as oil spill in a polar zone and leakage of high temperature oils because of its high thermal and chemical resistance.

CONCLUSIONS

In summary, a free-standing and flexible SiO_2−carbon composite nanofibrous membrane was fabricated by using electrospinning technique followed by thermal treatment. The bulk mechanical properties, that is, Young's modulus and toughness of the as-prepared membrane can be easily tuned by manipulating the SiO_2 loading. It is found that the composite membrane is tougher than the pristine CNF membrane when the embedded SiO_2 concentration is kept at 2.7 wt %, beyond which the membrane toughness is reduced. After coated with silicone oil, the composite membrane becomes ultra-hydrophobic and superoleophilic. The chemical and thermal stability test suggest that the wettability of the coated composite membrane is resistant to elevated temperature (up to 350 °C) and stable towards a wide range of pH values (2−14). Such wetting behavior allows the membrane to be applied as an substrate for separation of free water and oil. The quality test of oil-water separation shows that the membrane is highly effective in separating free oil and water. More importantly, the separation process is ultrafast and driven solely by gravity. We anticipate that this study will open up a new avenue for fabrication of free-standing carbonaceous composite membrane with tunable flexibility for energy-efficient, high-throughput production of purified water.

ASSOCIATED CONTENT

Supporting Information

Design of home-made solvent vapor jacket, images of electrospun pure SiO_2 nanofibers, images showing sequential process of water absorption by composite membrane, and videos. This material is available free of charge via the Internet at http://pubs.acs.org/.

AUTHOR INFORMATION

Corresponding Author

*Phone: (+65) 6790 627. Fax: (+65)-67910676. E-mail: ddsun@ntu.edu.sg.

Notes

The authors declare no competing financial interest.

ACKNOWLEDGMENTS

We would like to thank the lab technicians from Environment Lab and Central Environmental Science and Engineering (CESEL) lab in Nanyang Technological University (NTU) for technical support.

REFERENCES

(1) Zhang, J.; Seeger, S. Polyester Materials with Superwetting Silicone Nanofilaments for Oil/Water Separation and Selective Oil Absorption. *Adv. Funct. Mater.* **2011**, *21* (24), 4699−4704.

(2) Lee, C.; Baik, S. Vertically-Aligned Carbon Nanotube Membrane Filters with Superhydrophobicity and Superoleophilicity. *Carbon* **2010**, *48* (8), 2192−2197.

(3) Hejazi, V.; Nyong, A. E.; Rohatgi, P. K.; Nosonovsky, M. Wetting Transitions in Underwater Oleophobic Surface of Brass. *Adv. Mater.* **2012**, *24* (44), 5963−5966.

(4) Kota, A. K.; Li, Y.; Mabry, J. M.; Tuteja, A. Hierarchically Structured Superoleophobic Surfaces with Ultralow Contact Angle Hysteresis. *Adv. Mater.* **2012**, *24* (43), 5838−5843.

(5) Ji, J.; Fu, J.; Shen, J. Fabrication of a Superhydrophobic Surface from the Amplified Exponential Growth of a Multilayer. *Adv. Mater.* **2006**, *18* (11), 1441−1444.

(6) Zimmermann, J.; Rabe, M.; Artus, G. R. J.; Seeger, S. Patterned Superfunctional Surfaces Based on a Silicone Nanofilament Coating. *Soft Matter* **2008**, *4* (3), 450−452.

(7) Shang, Y.; Si, Y.; Raza, A.; Yang, L.; Mao, X.; Ding, B.; Yu, J. An In Situ Polymerization Approach for the Synthesis of Superhydrophobic and Superoleophilic Nanofibrous Membranes for Oil/Water Separation. *Nanoscale* **2012**, *4* (24), 7847−7854.

(8) Ding, B.; Li, C.; Hotta, Y.; Kim, J.; Kuwaki, O.; Shiratori, S. Conversion of an Electrospun Nanofibrous Cellulose Acetate Mat from a Superhydrophilic to Superhydrophobic Surface. *Nanotechnology* **2006**, *17* (17), 4332.

(9) Zhang, L.; Zhang, Z.; Wang, P. Smart Surfaces With Switchable Superoleophilicity and Superoleophobicity in Aqueous Media: Toward Controllable Oil/Water separation. *NPG Asia Mater.* **2012**, *4* (2), e8.

(10) Wang, C.; Yao, T.; Wu, J.; Ma, C.; Fan, Z.; Wang, Z.; Cheng, Y.; Lin, Q.; Yang, B. Facile Approach in Fabricating Superhydrophobic and Superoleophilic Surface for Water and Oil Mixture Separation. *ACS Appl. Mater. Interfaces* **2009**, *1* (11), 2613−2617.

(11) Ma, M.; Gupta, M.; Li, Z.; Zhai, L.; Gleason, K. K.; Cohen, R. E.; Rubner, M. F.; Rutledge, G. C. Decorated Electrospun Fibers Exhibiting Superhydrophobicity. *Adv. Mater.* **2007**, *19* (2), 255−259.

(12) Tang, X.; Si, Y.; Ge, J.; Ding, B.; Liu, L.; Zheng, G.; Luo, W.; Yu, J. In Situ Polymerized Superhydrophobic and Superoleophilic Nanofibrous Membranes for Gravity Driven Oil/water Separation. *Nanoscale* **2013**, *5* (23), 11657−11664.

(13) Calcagnile, P.; Fragouli, D.; Bayer, I. S.; Anyfantis, G. C.; Martiradonna, L.; Cozzoli, P. D.; Cingolani, R.; Athanassiou, A. Magnetically Driven Floating Foams for the Removal of Oil Contaminants from Water. *ACS Nano* **2012**, *6* (6), 5413−5419.

(14) Tian, D.; Zhang, X.; Wang, X.; Zhai, J.; Jiang, L. Micro/Nanoscale Hierarchical Structured ZnO Mesh Film for Separation of Water and Oil. *Phys. Chem. Chem. Phys.* **2011**, *13* (32), 14606−14610.

(15) Cheng, M.; Gao, Y.; Guo, X.; Shi, Z.; Chen, J.-f.; Shi, F. A Functionally Integrated Device for Effective and Facile Oil Spill Cleanup. *Langmuir* **2011**, *27* (12), 7371−7375.

(16) Kwon, G.; Kota, A.; Li, Y.; Sohani, A.; Mabry, J. M.; Tuteja, A. On-Demand Separation of Oil−Water Mixtures. *Adv. Mater.* **2012**, *24* (27), 3666−3671.

(17) Tan, W.; Yang, X. G.; Tan, X. F. Study on Demulsification of Crude Oil Emulsions by Microwave Chemical Method. *Sep. Sci. Technol.* **2007**, *42* (6), 1367−1377.
(18) Yang, H.; Pi, P.; Cai, Z.-Q.; Wen, X.; Wang, X.; Cheng, J.; Yang, Z.-r. Facile Preparation of Superhydrophobic and Superoleophilic Silica Film on Stainless Steel Mesh via Sol−Gel Process. *Appl. Surf. Sci.* **2010**, *256* (13), 4095−4102.
(19) Wang, Q.; Cui, Z.; Xiao, Y.; Chen, Q. Stable Highly Hydrophobic and Oleophilic Meshes for Oil/water Separation. *Appl. Surf. Sci.* **2007**, *253* (23), 9054−9060.
(20) Feng, L.; Zhang, Z.; Mai, Z.; Ma, Y.; Liu, B.; Jiang, L.; Zhu, D. A Superhydrophobic and Superoleophilic Coating Mesh Film for the Separation of Oil and Water. *Angew. Chem., Int. Ed.* **2004**, *43* (15), 2012−2014.
(21) Xue, Z.; Wang, S.; Lin, L.; Chen, L.; Liu, M.; Feng, L.; Jiang, L. A Novel Superhydrophilic and Underwater Superoleophobic Hydrogel-Coated Mesh for Oil/Water Separation. *Adv. Mater.* **2011**, *23* (37), 4270−4273.
(22) Gao, C.; Sun, Z.; Li, K.; Chen, Y.; Cao, Y.; Zhang, S.; Feng, L. Integrated Oil Separation and Water Purification by a Double-Layer TiO_2-Based Mesh. *Energy Environ. Sci.* **2013**, *6* (4), 1147−1151.
(23) Zhang, L.; Zhong, Y.; Cha, D.; Wang, P. A Self-Cleaning Underwater Superoleophobic Mesh for Oil/Water Separation. *Sci. Rep.* **2013**, *3*, 2326.
(24) Zhang, F.; Zhang, W. B.; Shi, Z.; Wang, D.; Jin, J.; Jiang, L. Nanowire-Haired Inorganic Membranes with Superhydrophilicity and Underwater Ultralow Adhesive Superoleophobicity for High-Efficiency Oil/Water Separation. *Adv. Mater.* **2013**, *30*, 4192−4198.
(25) Chen, W.; Su, Y.; Zheng, L.; Wang, L.; Jiang, Z. The Improved Oil/Water Separation Performance of Cellulose Acetate-Graft-Polyacrylonitrile Membranes. *J. Membrane Sci.* **2009**, *337* (1−2), 98−105.
(26) Cheryan, M.; Rajagopalan, N. Membrane Processing of Oily Streams. Wastewater Treatment and Waste Reduction. *J. Membrane Sci.* **1998**, *151* (1), 13−28.
(27) Hlavacek, M. Break-Up of Oil-in-Water Emulsions Induced by Permeation Through a Microfiltration Membrane. *J. Membrane Sci.* **1995**, *102* (0), 1−7.
(28) Maphutha, S.; Moothi, K.; Meyyappan, M.; Iyuke, S. E. A Carbon Nanotube-Infused Polysulfone Membrane with Polyvinyl Alcohol Layer for Treating Oil-Containing Waste Water. *Sci. Rep.* **2013**, *3*, 1509.
(29) Mohammadi, T.; Kazemimoghadam, M.; Saadabadi, M. Modeling of Membrane Fouling and Flux Decline in Reverse Osmosis during Separation of Oil in Water Emulsions. *Desalination* **2003**, *157* (1−3), 369−375.
(30) Pan, Y.; Wang, W.; Wang, T.; Yao, P. Fabrication of Carbon Membrane and Microfiltration of Oil-in-Water Emulsion: An Investigation on Fouling Mechanisms. *Sep. Purif. Technol.* **2007**, *57* (2), 388−393.
(31) Arnot, T. C.; Field, R. W.; Koltuniewicz, A. B. Cross-Flow and Dead-End Microfiltration of Oily Water Emulsions. Part II. Mechanisms and Modelling of Flux Decline. *J. Membrane Sci.* **2000**, *169* (1), 1−15.
(32) Pang, L. S. K.; Saxby, J. D.; Chatfield, S. P. Thermogravimetric Analysis of Carbon Nanotubes and Nanoparticles. *J. Phys. Chem.* **1993**, *97* (27), 6941−6942.
(33) Muramatsu, H.; Hayashi, T.; Kim, Y. A.; Shimamoto, D.; Kim, Y. J.; Tantrakarn, K.; Endo, M.; Terrones, M.; Dresselhaus, M. S. Pore Structure and Oxidation Stability of Double-Walled Carbon Nanotube-Derived Bucky Paper. *Chem. Phys. Lett.* **2005**, *414* (4-6), 444−448.
(34) Zhai, Y.; Dou, Y.; Zhao, D.; Fulvio, P. F.; Mayes, R. T.; Dai, S. Carbon Materials for Chemical Capacitive Energy Storage. *Adv. Mater.* **2011**, *23* (42), 4828−4850.
(35) Shi, Z.; Zhang, W.; Zhang, F.; Liu, X.; Wang, D.; Jin, J.; Jiang, L. Ultrafast Separation of Emulsified Oil/Water Mixtures by Ultrathin Free-Standing Single-Walled Carbon Nanotube Network Films. *Adv. Mater.* **2013**, *17*, 2422−2427.
(36) Lee, C. H.; Johnson, N.; Drelich, J.; Yap, Y. K. The Performance of Superhydrophobic and Superoleophilic Carbon Nanotube Meshes in Water−Oil Filtration. *Carbon* **2011**, *49* (2), 669−676.
(37) Kracke, B.; Damaschke, B. Measurement of Nanohardness and Nanoelasticity of Thin Gold Films with Scanning Force Microscope. *Appl. Phys. Lett.* **2000**, *77* (3), 361−363.
(38) Ko, F.; Gogotsi, Y.; Ali, A.; Naguib, N.; Ye, H.; Yang, G.; Li, C.; Willis, P. Electrospinning of Continuous Carbon Nanotube-Filled Nanofiber Yarns. *Adv. Mater.* **2003**, *15* (14), 1161−1165.
(39) Mack, J. J.; Viculis, L. M.; Ali, A.; Luoh, R.; Yang, G.; Hahn, H. T.; Ko, F. K.; Kaner, R. B. Graphite Nanoplatelet Reinforcement of Electrospun Polyacrylonitrile Nanofibers. *Adv. Mater.* **2005**, *17* (1), 77−80.
(40) Choi, S.-S.; Lee, S.; Im, S.; Kim, S.; Joo, Y. Silica Nanofibers from Electrospinning/Sol−Gel Process. *J. Mater. Sci. Lett.* **2003**, *22* (12), 891−893.
(41) Liu, Y.; Sagi, S.; Chandrasekar, R.; Zhang, L.; Hedin, N. E.; Fong, H. Preparation and Characterization of Electrospun SiO_2 Nanofibers. *J. Nanosci. Nanotechnol.* **2008**, *8* (3), 1528−1536.
(42) Woo, S.-W.; Dokko, K.; Nakano, H.; Kanamura, K. Preparation of Three Dimensionally Ordered Macroporous Carbon with Mesoporous Walls for Electric Double-Layer Capacitors. *J. Mater. Chem.* **2008**, *18* (14), 1674−1680.
(43) Yan, X.; Tai, Z.; Chen, J.; Xue, Q. Fabrication of Carbon Nanofiber-Polyaniline Composite Flexible Paper for Supercapacitor. *Nanoscale* **2011**, *3* (1), 212−216.
(44) Wang, P.; Du, M.; Zhang, M.; Zhu, H.; Bao, S. The Preparation of Tubular Heterostructures Based on Titanium Dioxide and Silica Nanotubes and Their Photocatalytic Activity. *Dalton Trans.* **2014**, *43* (4), 1846−1853.
(45) Patel, A. C.; Li, S.; Wang, C.; Zhang, W.; Wei, Y. Electrospinning of Porous Silica Nanofibers Containing Silver Nanoparticles for Catalytic Applications. *Chem. Mater.* **2007**, *19* (6), 1231−1238.
(46) Si, M.; Feng, D.; Qiu, L.; Jia, D.; Elzatahry, A. A.; Zheng, G.; Zhao, D. Free-Standing Highly Ordered Mesoporous Carbon-Silica Composite Thin Films. *J. Mater. Chem. A* **2013**, *1* (43), 13490−13495.
(47) Zhuravlev, L. T. The Surface Chemistry of Amorphous Silica. Zhuravlev Model. *Colloid Surface. A* **2000**, *173* (1−3), 1−38.
(48) Sakka, S.; Kamiya, K. The Sol−Gel Transition in the Hydrolysis of Metal Alkoxides in Relation to the Formation of Glass Fibers and Films. *J. Non-Cryst. Solids* **1982**, *48* (1), 31−46.
(49) Novak, B. M. Hybrid Nanocomposite Materials—Between Inorganic Glasses and Organic Polymers. *Adv. Mater.* **1993**, *5* (6), 422−433.
(50) Liu, Y.-L.; Wei, W.-L.; Hsu, K.-Y.; Ho, W.-H. Thermal Stability of Epoxy-Silica Hybrid Materials by Thermogravimetric Analysis. *Thermochim. Acta* **2004**, *412* (1−2), 139−147.
(51) Chen, Y.; Iroh, J. O. Synthesis and Characterization of Polyimide/Silica Hybrid Composites. *Chem. Mater.* **1999**, *11* (5), 1218−1222.
(52) Cebeci, F. Ç.; Wu, Z.; Zhai, L.; Cohen, R. E.; Rubner, M. F. Nanoporosity-Driven Superhydrophilicity: A Means to Create Multifunctional Antifogging Coatings. *Langmuir* **2006**, *22* (6), 2856−2862.
(53) Shirtcliffe, N. J.; McHale, G.; Newton, M. I.; Perry, C. C.; Roach, P. Porous Materials Show Superhydrophobic to Superhydrophilic Switching. *Chem. Commun.* **2005**, *25*, 3135−3137.
(54) Chen, P. C.; Xu, Z. K. Mineral-Coated Polymer Membranes with Superhydrophilicity and Underwater Superoleophobicity for Effective Oil−Water Separation. *Sci. Rep* **2013**, *3*, 2776.
(55) Zhang, W.; Shi, Z.; Zhang, F.; Liu, X.; Jin, J.; Jiang, L. Superhydrophobic and Superoleophilic PVDF Membranes for Effective Separation of Water-in-Oil Emulsions with High Flux. *Adv. Mater.* **2013**, *25* (14), 2071−2076.
(56) Ju, H.; McCloskey, B. D.; Sagle, A. C.; Wu, Y.-H.; Kusuma, V. A.; Freeman, B. D. Crosslinked Poly(Ethylene Oxide) Fouling Resistant Coating Materials for Oil−Water Separation. *J. Membrane Sci.* **2008**, *307* (2), 260−267.

(57) Chakrabarty, B.; Ghoshal, A. K.; Purkait, M. K. Ultrafiltration of Stable Oil-in-Water Emulsion by Polysulfone Membrane. *J. Membrane Sci.* **2008**, *325* (1), 427−437.
(58) Mueller, J.; Cen, Y.; Davis, R. H. Crossflow Microfiltration of Oily Water. *J. Membrane Sci.* **1997**, *129* (2), 221−235.